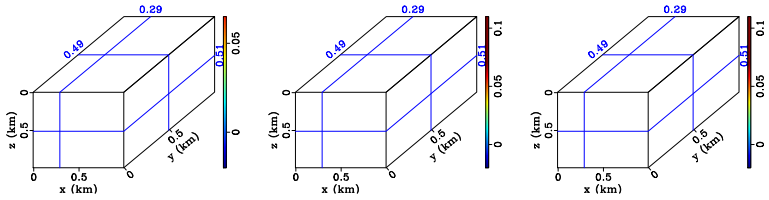

Figure 2 *Actual weaknesses $\triangle_N$ (left), $\triangle_V$ (middle), and $\triangle_H$ (right).*

across two other fracture sets are shown in Figures 4 and 5, respectively. As expected, fractures located near the edge of the model are inverted with a lower resolution compared to those close to the center.

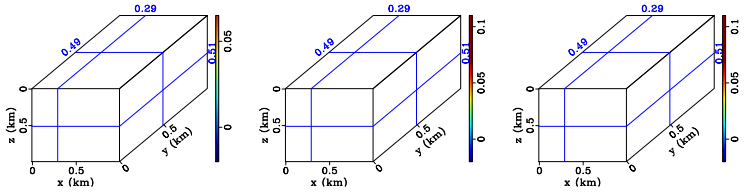

Figure 3 *Inverted $\triangle_N$ (left), $\triangle_V$ (middle), and $\triangle_H$ (right). The sweet spot near the center of the model is successfully resolved.*

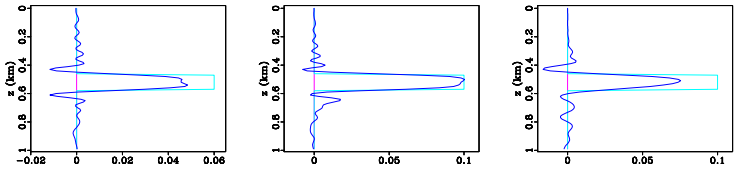

Figure 4 *Vertical profiles of $\triangle_N$ (left), $\triangle_V$ (middle), and $\triangle_H$ (right) at point ($x = 0{:}5$ km; $y = 0{:}5$ km). Cyan: actual model; Pink: initial model; Blue: inverted model.*

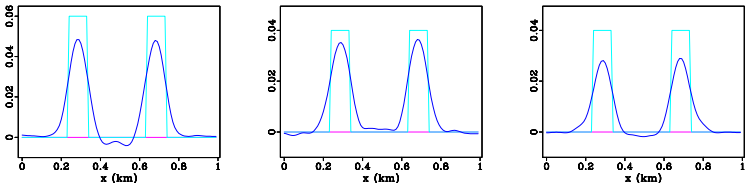

Figure 5 *Horizontal profiles of $\triangle_N$ (left), $\triangle_V$ (middle), and $\triangle_H$ (right) at point ($z = 0{:}47$ km; $y = 0{:}7$ km). Cyan: actual model; Pink: initial model; Blue: inverted model.*

Figure 6 *Azimuthally varying radiation patterns of the incident P-wave and reflected P-wave (top) / SH-wave (bottom) for the fracture weaknesses. The radial direction indicates the opening angle. The P-SV wave (not shown) has a behavior similar to that of P-P wave.*

To better understand the inversion results, Figure 6 shows the radiation scattering patterns of the fracture weaknesses (Oh and Alkhalifah, 2016). The parameters $\triangle_N$ and $\triangle_H$ are more sensitive to large opening angles and, therefore, need large offset-to-depth ratios to be resolved. The weakness $\triangle_V$ is more sensitive to medium opening angles, so it can be inverted with a high resolution from conventional-spread

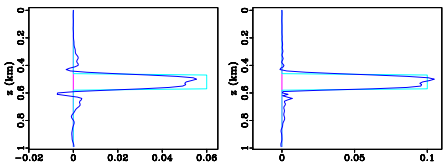

Figure 7 *Vertical profiles of the normal weakness (left) and tangential weakness (right) of penny-shaped cracks. Cyan: actual model; Pink: initial model; Blue: inverted model.*

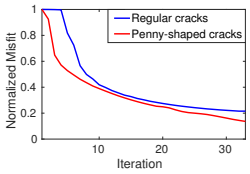

Figure 8 *Normalized misfit functions vs. iteration for the last frequency band (0-21 Hz).*

data. Since only one tangential weakness can be resolved with surface acquisition, next we assume the model of penny-shaped cracks, which have the same vertical and horizontal tangential weaknesses ($\triangle_V = \triangle_H$). As illustrated by the estimated weaknesses in Figure 7, the inversion for penny-shaped cracks provides a more accurate normal weakness (further improvement in $\triangle_N$ can be achieved by including larger offsets) and a well-resolved tangential weakness. Using the simpler crack model provides comprable rate of convergence (Figure 8) in this limited offset example.

Conclusions

We proposed a new approach to estimate the spatial distribution and physical properties of fractures by waveform inversion of multicomponent surface data. Due to the high-resolution potential of elastic full waveform inversion involved in the scattering components of the data, the developed algorithm can recover the spatial fracture distribution and identify localized "sweet spots" of intense fracturing. The numerical example also shows that the vertical tangential weakness $\triangle_V$ is better resolved than the other two weaknesses. The radiation patterns indicate that reliable estimation of the normal weakness $\triangle_N$ requires a relatively large offset-to-depth ratio. The weakness $\triangle_H$ cannot be obtained with sufficient accuracy, which is also confirmed by previous studies. A shape-regularization term is added to the objective function to improve the quality of the inverted parameter $\triangle_H$. Alternatively, the simplified model of penny-shaped cracks, often employed in practice, yields good inversion results and comparable convergence for this limited offset data. The proposed method has the same limitations as more conventional FWI algorithms: it requires a good background model and sufficient subsurface illumination.

Acknowledgements

We thank Juwon Oh, Ramzi Djebbi, Nabil Masmoudi and Yike Liu (IGG, CAS) for their helpful discussions. For computer time, this research used the resources of the Supercomputing Laboratory at King Abdullah University of Science & Technology (KAUST) in Thuwal, Saudi Arabia.

References

Bakulin, A., Grechka, V. and Tsvankin, I. [2000a] Estimation of fracture parameters from reflection seismic data-Part I: HTI model due to a single fracture set. *Geophysics*, **65**(6), 1788–1802.

Bakulin, A., Grechka, V. and Tsvankin, I. [2000b] Estimation of fracture parameters from reflection seismic data-Part II: Fractured models with orthorhombic symmetry. *Geophysics*, **65**(6), 1803–1817.

Gallardo, L.A. and Meju, M.A. [2003] Characterization of heterogeneous near-surface materials by joint 2D inversion of dc resistivity and seismic data. *Geophysical Research Letters*, **30**(13).

Masmoudi, N., Tsvankin, I. and Alkhalifah, T. [2016] Feasibility of high-resolution fracture characterization using waveform inversion. In: *78th EAGE Conference and Exhibition 2016*.

Oh, J.W. and Alkhalifah, T. [2016] Elastic orthorhombic anisotropic parameter inversion: An analysis of parameterization. *Geophysics*, **81**(6), C279–C293.

Schoenberg, M. [1980] Elastic wave behavior across linear slip interfaces. *The Journal of the Acoustical Society of America*, **68**(5), 1516–1521.

Tsvankin, I. and Grechka, V. [2011] *Seismology of azimuthally anisotropic media and seismic fracture characterization*. Society of Exploration Geophysicists.